Tenth International Conference on Computational Fluid Dynamics (ICCFD10), Barcelona,Spain, July 9-13, 2018

ICCFD10-2018-0123

Compact Interface quasi-Newton algorithm for biomechanical applications in massively parallel computers

A. Santiago*, J. Aguado-Sierra*, E. Casoni*, R. Arís*, G. Houzeaux*, M. Vázquez*,**
Corresponding author: alfonso.santiago@bsc.es

* ,Barcelona Supercomputing Center (BSC), Barcelona, Spain.
** IIIA-CSIC, Bellaterra, Spain.

Abstract: In this work we present aHPC version of the interface quasi Newton algorithm. This algorithm is used to couple staggered fluid-structure interaction (FSI) solvers. This algorithm allows to tackle two of the main problems in computational biomechanics: added mass instability and n-fieldcoupling. The components of the IQN algorithm are dismembered and fused to obtain a reduced version, minimizing memory consumption and operations. This algorithm is firstly tested with a complex 2D case, and after used to compute a whole heart. The fluid-electro-mechanical model computed in the whole heart, provided deeper insights in the heartbeat behavior. Although the intracavitary velocities are smaller, the Q-criterion analysis revealed a more complex fluid pattern, if compared against the outflow tracts. Although the limitations of this model, this work is a step forward a simulation tool to study physiopathology and test biomedical devices.

Keywords: Fluid Structure Interaction, Biomechanics, cardiac modelling.

1 Introduction

Although *in vivoin vitro* experiments is essential to improve biomedical research, computational tools are gradually gaining importance. Biomechanical simulations provide a powerful tool [4, 5, 6] to understand heart function and its behavior under congenital [7, 8] and acquired pathologies [9, 10, 11]. Besides this, and as happens in other disciplines, simulations can become a key tool in designing surgical procedures, techniques or devices. However, modelling the beating heart and its pumping action is a highly complex task. In the heartbeat, different types of physical problems are involved. In the muscle, the electrical stimuli propagates through the cardiac myocytes causing the cardiac muscle contraction[12, 13], which in turn exerts work upon the blood inside the cavities. Therefore, from the computational mechanics standpoint, the heartbeat is a tightly coupled fluid-electro-mechanical problem.

Nowadays, there is no review paper that deeply analyzes three-physics models of the heart, to the authors knowledge. The reason for this is, probably, the scarcity of such models. Despite this, partial reviews can be found in [14, 15, 16]. These fluid-electro-mechanical models solve the three set of equations in a coupled manner. Despite the work done in experimental and computational research of multiphysics heart modelling [15], there is no reference of a tightly-coupled scheme that includes electrophysiology, solid and fluid mechanics in a whole human heart. A bidirectional fluid-structure interaction (FSI) coupling is consistently seen is models that does not include electrophysiology, but is not usual in three-physics models. In this last group, the usual FSI approach is one-way scheme, where electro-mechanical action imposes the displacement to the fluid mechanics without feedback from the fluid to the solid. This is why a robust FSI method is mandatory to obtain such type of three-physics models. The FSI problem present in the heart is specially complex for two main reasons. First, as the densities of the fluid (ρ^f) and the solid ρ^s are similar, added mass instability [2] may arise. Second, the heart have two independent FSI problems that should be solved at the same time: the left and the right sides.

Two main methods are available to tackle the FSI problem: the monolithic and the partitioned approaches. In the former, flow and structure are solved simultaneously and, hence, the interaction between both domains is taken into account during the solution process. In the latter, flow is solved separately from structure, requiring a coupling algorithm that deals with the interaction between both domains [17]. As the monolithic approach treat both domains as a single problem, no coupling iterations between the fluid and the structure are required in each time step. On the contrary, with the partitioned approach, the flow and the structure equations have to be solved in each coupling iteration until convergence. The main advantage of the partitioned approach is that it can reuse reliable and optimized codes to solve both sets of equations. This makes the partitioned approach modular and easier to maintain. Also, flow and structure can be solved with different techniques, particularly suited for each kind of equations. Conversely, monolithic codes typically solve all the equations with the same solution technique, facing the challenging problem of preconditioning the matrix in such way that allows to converge both problems simultaneously. Partitioned coupling schemes can be also classified in weakly (also known as loosely or explicit) and strongly (also known as implicit) coupling. The former solves flow and structure only once per time step, therefore equilibrium of the interface variables are not ensured. On the latter, convergence is achieved once there is continuity of the coupling variables. For a further comparison between monolithic and partitioned approaches, please refer to [18].

In this work, we present a robust FSI algorithm optimized to run in supercomputers, that tackles both main problems of FSI in biomechanics. This novel method allows to solve the three-physics problem of the heartbeat.

2 Methods

2.1 General overview of the problem and common computational aspects

From a physical standpoint, the heart pumping action can be decomposed in three coupled problems: the propagation of the action potential that induces the mechanical deformation of the solid and which in turn performs work against the fluid (1). The two coupling points are electro-mechanical and fluid-structure, both of them bi-directional.

The four problems share some common features, described below. All of them are implemented and solved in Alya, the BSC's in-house parallel simulation code for coupled multi-physics problems [19, 20, 21, 22, 23]. The four problems are discretized in space using the Finite Element Method (FEM) on non-structured meshes, and in time using Finite Diferences Method (FDM). Once discretized, the continuum mechanics models are transformed in algebraic systems. Non-linear problems are linearized and solved either with Jacobi (*i.e.* fixed point) or Newton iterations. We describe below the strategy for each problem.

The coupled problem is solved following a multi-code approach, especially well-suited for staggered coupling. The simulation problem is split in two sub-problems: tissue and blood inside the cavities, being each of the sub-problems solved with a separate Alya instance (for a graphical reference refer to figure 1). Each of the sub-problems the two instances simulates are usually large and, therefore, parallelized using domain decomposition.

2.2 Single physics governing equation

2.2.1 Electrophysiology

The computational electrophysiology (EP) scheme used is originally introduced in [20].The EP problem is decomposed in tissue and cell models. The tissue is solved using a monodomain model, which is governed by an anisotropic diffusion equation. The cell model is plugged to the tissue model as a non-linear Ordinary Differential Equation (ODE) system. The cell model is specifically designed from single cell experiments, with a wide range of complexity degree and application ranges [24, 25, 26, 25, 27, 28]. The EP models

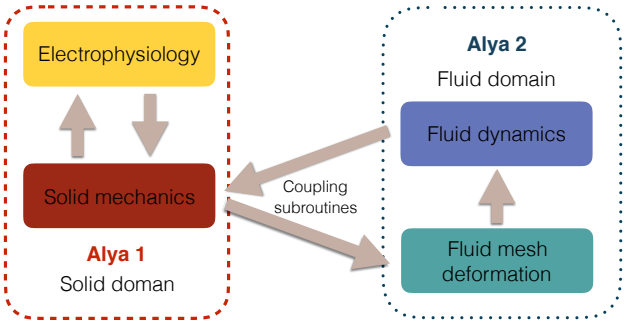

Figure 1: Model overview. Two bidirectionally coupled problems: electro-mechanical and fluid-structure one, with three systems of equations describing them: electrophysiology, solid mechanics, and fluid mechanics in deformable mesh.

general form is as follows:

$$\begin{aligned} C_m \frac{d\phi}{dt} + I_{\text{ion}}(\phi, \mathbf{w}, \mathbf{c}) &= I_{\text{app}}(t) \\ \frac{d\mathbf{w}}{dt} &= m_w(\phi, \mathbf{w}, \mathbf{c}) \\ \frac{d\mathbf{c}}{dt} &= m_c(\phi, \mathbf{w}, \mathbf{c}) \end{aligned} \tag{1}$$

where ϕ is the activation potential and C_m the membrane capacitance. $I_{\text{app}}(t)$ is the applied current, typically used to impose an initial activation. I_{ion} is the ionic currents term, a sum of all the P ionic currents considered and whose form depends on the cell model. $\mathbf{w}$ and $\mathbf{c}$ are respectively the M gating variables and the P intracellular concentrations of each of the P ionic currents. In this work we use the O'Hara-Rudy cell model [28] for human ventricles.

2.2.2 Solid mechanics

Lets define X_j a material point in the reference configuration and x_i the corresponding point in the deformed configuration. The equation of balance of momentum with respect to the reference configuration can be written as:

$$\rho^s \frac{\partial^2 u_i}{\partial t^2} = \frac{\partial P_{ji}}{\partial X_j} + \rho^s b_i, \tag{2}$$

where u_i is the unknown, ρ^s is the tissue density (with respect to the reference volume). Tensor P_{ji} and vector b_i stand for, respectively, the first Piola-Kirchoff (nominal stress) and the distributed body force in the undeformed configuration. The Cauchy stress $\boldsymbol{\sigma} = J^{-1}\boldsymbol{P}\boldsymbol{F}^{\mathrm{T}}$, is related to the nominal stress through the the deformation gradient tensor $F_{ij} = \partial x_i / \partial X_j$. $J = \det(\boldsymbol{F})$ is the Jacobian determinant. In cardiac tissue models [29], stress is assumed to be a combination of passive and active parts:

$$\boldsymbol{\sigma} = \boldsymbol{\sigma}_{pas} + \boldsymbol{\sigma}_{act}(\lambda, [Ca^{2+}])\boldsymbol{f} \otimes \boldsymbol{f}, \tag{3}$$

where $\boldsymbol{f} = f_i$ is the normalised vector along the fibres. Following [30] the passive part is modelled as a slightly compressible, elastic, invariant-type material [30] and through a transverse isotropic exponential strain energy function $W(\boldsymbol{b})$.

The depolarization of the cell membrane triggers the mechanical deformation of the myocytes, modelled as the stress active part ($\boldsymbol{\sigma}_{act}$ in eqn 3). In this paper we use a Hunter-McCulloch model [31], which assumes that the active stress is produced only in the direction of the fibre and depends on the Calcium concentration of the cardiac cell:

$$\sigma_{act} = \frac{[Ca^{2+}]^n}{[Ca^{2+}]^n + C_{50}^n} \sigma_{max}(1 + \beta(\lambda_f - 1)). \tag{4}$$

where C_{50} is the Calcium concentration for 50% of σ^{max}, n is a coefficient that controls the shape of the curve, σ^{max} is the maximum tensile stress generated at the maximum extension ratio $\lambda = 1$ and β is a parameter that scales the active stress produced.

2.2.3 Fluid dynamics in a deformable mesh

Computational fluid dynamics (CFD) inside cavities and vessels is modelled by the incompressible flow Navier-Stokes equations for a Newtonian fluid on a deformable mesh using an Aritrary Lagrangian-Eulerian (ALE) scheme. Flow equations are:

$$\rho^f \frac{\partial u_i}{\partial t} + \rho^f \left(u_j - u_j^m\right) \frac{\partial u_i}{\partial x_j} + \frac{\partial}{\partial x_j}\left[+p\delta_{ij} - \mu\left(\frac{\partial u_i}{\partial x_j} + \frac{\partial u_j}{\partial x_i}\right)\right] = \rho^f f_i \tag{5}$$

$$\frac{\partial u_i}{\partial x_i} = 0, \tag{6}$$

where μ is the viscosity, ρ^f is the fluid density, u_i is the velocity, p is the mechanical pressure and u_j^m is the mesh velocity.

The numerical model is based on FEM for space and FDM for the time, using the Variational Multi Scale (VMS) technique [32] to stabilize convection and pressure. In order to solve this system efficiently in supercomputers, a split approach is used [19].

The ALE scheme requires the solution of another discretized partial differential equation for the mesh movement. We use the technique proposed in [33], where the mesh movement is governed by the following Laplacian equation:

$$\frac{\partial}{\partial x_j}\left(\left[1 + \alpha^e\right] \frac{\partial b_i}{\partial x_j}\right) = 0, \tag{7}$$

which is solved using FEM to discretize the space. In this equation, b_i are the components of the displacement at each point for the domain. The factor α^e controls the mesh distortion depending on the minimum and maximum element volumes in the mesh.

2.3 Fluid structure interaction

2.3.1 Continuity conditions and computational scheme

Mechanical deformation and fluid dynamics is coupled at the the wet surface, which is the contact boundary or interface between blood (simulated using CFD) and tissue (simulated using CSM). At the discrete level, continuity of displacements (${}^{\text{CFD}}d_i^{\Gamma_c}$, ${}^{\text{CSM}}d_i^{\Gamma_c}$) and normal stresses (${}^{\text{CSM}}\sigma_{ij}^{\Gamma_c} n_j$, ${}^{\text{CFD}}\sigma_{ij}^{\Gamma_c} n_j$) for CFD and CSM respectively, in the wet surface Γ_c must be enforced:

$$\begin{aligned} {}^{\text{CFD}}d_i^{\Gamma_c} &= {}^{\text{CSM}}d_i^{\Gamma_c} \\ {}^{\text{CFD}}\sigma_{ij}^{\Gamma_c} n_j &= {}^{\text{CSM}}\sigma_{ij}^{\Gamma_c} n_j, \end{aligned} \tag{8}$$

The normal stresses ${}^{\text{CFD}}\sigma_{ij}^{\Gamma_c} n_j$ are translated as a surface force applied in the contact boundary Γ_c as:

$$g_i = {}^{\text{CFD}}\sigma_{ij}^{\Gamma_c} n_j, \tag{9}$$

where n_j is the normal to the surface. The mesh is constructed to be conforming, having coincident nodes at Γ_c, avoiding interpolation approximations that may lead to non-conservativeness of the coupling variables.

Although the CSM is solved altogether with the EP problem, for the sake of clearness, the EP set of equation is avoided in this section. Anyway, after this problem is included, all said here stands, as it does not forms part of the FSI problem. Briefly explained, the domain is split in the fluid and solid domains with a Dirichlet-Neumann decomposition approach. In this way, the CSM problem can be defined as $d_\alpha^{I+1} = CSM(f_\alpha)$ and the CFD problem as $f_\alpha^{I+1} = CFD(d_\alpha)$, where the Greek subindex represents the degrees of freedom (dof). With this, the fixed-point algorithm for each iteration can be written as:

$$d_\alpha^{I+1} = \text{CSM}(\text{CFD}(d_\alpha)) \tag{10}$$

or as:

$$f_\alpha^{I+1} = \text{CFD}(\text{CSM}(f_\alpha)) \tag{11}$$

depending on the order the solvers are computed. To obtain convergence of the interface variables, iterations inside each time step are required:

while *Time loop* **do**
  $d_\alpha = d_\alpha^{ini}$
  while *Coupling loop* **do**
    $d_\alpha = \text{CSM}(f_\alpha)$
    $f_\alpha = \text{CFD}(d_\alpha)$
    $f_\alpha^{I+1} = \varphi_{GS}(f_\alpha)$
  end
end

Algorithm 1: FSI computational scheme. φ_{GS} represents the relaxation algorithm, d_α and f_α the displacements and forces in the interface.

In algorithm 1 the CSM and CFD problems are solved in a block manner way, although each one of the solvers are running in multiple cores. the φ_{GS} function modifies the unknown before computing the next iteration. The objective of this step is to accelerate convergence. Several relaxation schemes were developed in the past as the Aitken [34] or the Broyden [35] methods. In this work, modify the interface quasi-Newton (IQN) method proposed in [1].

2.3.2 The interface quasi-newton algorithm

In a generic manner, the problem in equations 10 and 11 can be stated as $\tilde{x}_\alpha = H(x_\alpha)$. We can define the next iterate as $x_\alpha^{I+1} = \tilde{x}_\alpha + \Delta x_\alpha$. The unknown increment Δx_α can be approximated as:

$$\Delta x_\alpha = W_{\alpha i}\lambda_i. \tag{12}$$

Where $W_{\alpha i}$ is:

$$W_{\alpha i} = \left[\Delta\widetilde{x}_\alpha^{I-1}, \Delta\widetilde{x}_\alpha^{I-2}, ..., \Delta\widetilde{x}_\alpha^{0}\right], \tag{13}$$

as a matrix containing in each column the unknown increments $\Delta\tilde{x}_\alpha^{I-1} = \tilde{x}_\alpha^{I-1} - \tilde{x}_\alpha$. Finally λ_i is obtained by solving the following problem:

$$V_{\alpha j}\lambda_j = r_\alpha, \tag{14}$$

where $r_\alpha = \tilde{x}_\alpha - x_\alpha$ is the residue for the interface problem and $V_{\alpha j}$ is:

$$V_{\alpha i} = \left[\Delta r_\alpha^{I-1}, \Delta r_\alpha^{I-2}, ..., \Delta r_\alpha^{0}\right], \tag{15}$$

a matrix containing in each column the residual increments for the interface problem $\Delta r_\alpha^{I-1} = r_\alpha^{I-1} - r_\alpha$. To solve eqn. 14 the matrix $V_{\alpha i}$ is decomposed by a QR decomposition, where an orthogonal matrix $Q_{\alpha\beta}$ and an upper triangular $U_{\alpha i}$ are obtained:

$$V_{\alpha i} = Q_{\alpha\beta}U_{\beta i}. \tag{16}$$

After this decomposition, the vector λ_i can be built by backsubstitution of the upper triangular matrix U_{ij}:

$$U_{ij}\lambda_j = Q_{\alpha i}\Delta r_\alpha. \tag{17}$$

As $\Delta r_\alpha = r_\alpha^{I-1} - r_\alpha$ and the objective is to get $\Delta r_\alpha = 0_\alpha - r_\alpha$, we can say:

$$U_{ij}\lambda_j = -Q_{\alpha i}r_\alpha. \tag{18}$$

As $Q_{\alpha i}$ is orthogonal, the inverse is equal to the transpose, avoiding the inversion of this matrix. Also, As U_{ij} is upper triangular, obtaining λ_i is trivial. Once λ_i is computed, the increment of the unknown Δx_α can

be computed as $\Delta x_\alpha = W_{\alpha i}\lambda_i$, and the update of the unknown as:

$$x_\alpha^{I+1} = \widetilde{x}_\alpha + W_{\alpha i}\lambda_i. \tag{19}$$

Although after eqn. 18 is the algorithm is computationally cheap, obtaining the $Q_{\alpha\beta}$ and and $U_{\alpha i}$ through the QR decomposition is a computational and memory expensive task.

2.3.3 High performance QR-decomposition

The QR decomposition by Householder reflections can be seen as a change of base, from a linearly independent set of vectors sorted in a matrix, to an orthogonal base of the original matrix. The goal is to obtain the orthogonal matrix $Q_{\alpha\beta}$ and the upper triangular matrix $U_{\alpha i}$, with the following shape:

$$Q_{\alpha\epsilon} = {}^1B_{\alpha\beta}\ {}^2B_{\beta\gamma}...\ {}^qB_{\gamma\epsilon} \tag{20}$$

$$U_{\alpha i} = {}^qB_{\alpha\beta}...\ {}^2B_{\beta\gamma}\ {}^1B_{\gamma\epsilon}V_{\epsilon i}, \tag{21}$$

where $B_{\alpha\beta}$ are intermediate matrices obtained during the iterative decomposition. As $Q_{\alpha\epsilon}$ in eqn. 20 is used in eqn. 18 we can reforumlate eqn 20 as:

$$Q_{\alpha\epsilon} = {}^1B_{\alpha\beta}\ {}^2B_{\beta\gamma}...\ {}^qB_{\gamma\epsilon}r_\alpha \tag{22}$$

to compute both $Q_{\alpha\epsilon}$ and $U_{\alpha i}$ from right to left and reduce the operations to matrix-vector products avoiding intermediate dense matrices. This structure of $V_{\alpha i}$ can be considered as a set of q ordered vectors:

$$V_{\alpha i} = \left[\begin{bmatrix} v_{11} \\ v_{21} \\ \vdots \end{bmatrix} \quad \begin{bmatrix} v_{12} \\ v_{22} \\ \vdots \end{bmatrix} \quad \cdots \quad \begin{bmatrix} v_{1q} \\ v_{2q} \\ \vdots \end{bmatrix} \right] = [v_{\alpha 1}, v_{\alpha 2}, \cdots, v_{\alpha q}] = {}^1V_{\alpha i}. \tag{23}$$

At each of these iterations, the matrix $V_{\alpha i}$ is modified column by column. The QR decomposition iteratively makes each column orthogonal to the original base and to each other column in the matrix. The QR decomposition starts iteration j with a matrix ${}^jV_{\alpha i}$ obtained with data from iteration $j-1$. To decompose the $j-th$ column of ${}^jV_{\alpha i}$, a unitary vector u_α has to be built:

$$u_\alpha = \frac{n_\alpha}{\|n_\alpha\|} \quad \text{with,} \quad n_\alpha = v_\alpha - \|v_\alpha\|\ {}^je_\alpha, \tag{24}$$

where v_α is the column to decompose and ${}^je_\alpha$ is a unitary vector with $j-th$ position equal to 1 and to 0 otherwise. Then,

$${}^jB^*_{\alpha\beta} = \delta_{\alpha\beta} - 2u_\alpha u_\beta \tag{25}$$

is the Householder matrix associated to the original plane, and $\delta_{\alpha\beta}$ is the identity matrix. If the matrix ${}^jV_{\alpha i}$ is premultiplied by ${}^jB^*_{\alpha\beta}$, a new matrix ${}^jB^*_{\alpha\beta}\ {}^jV_{\beta i}$ is obtained. The resulting matrix is upper triangular in all the j first columns; and dense everywhere else. In order to properly compute eqn. 22, matrices ${}^jB_{\alpha i}$ are filled with the identity:

$${}^jB_{\alpha i} = \begin{bmatrix} I_{ij} & 0 \\ 0 & {}^jB^*_{\alpha i} \end{bmatrix} \tag{26}$$

where $I_{ij} \in \mathbb{R}^{j-1\times j-1}$.

To improve computing and memory cost, we propose some modifications for the already modified algorithm. As ${}^jB_{\alpha\beta}$ is obtained by the relation eqn 25, the products ${}^jB_{\alpha\beta}\ {}^jV_{\beta i}$ and ${}^qB_{\alpha\beta}r_\alpha$ can be expanded as:

$${}^jB_{\alpha\beta}\ {}^jV_{\beta i} = (\delta_{\alpha\beta} - 2u_\alpha u_\beta)\ {}^jV_{\beta i} = {}^jV_{\alpha i} - 2u_\alpha u_\beta\ {}^jV_{\beta i}. \tag{27}$$

$${}^qB_{\alpha\beta}r_\alpha = (\delta_{\alpha\beta} - 2\ {}^qu_\alpha\ {}^qu_\beta)r_\beta = r_\beta - 2\ {}^qu_\alpha\ {}^qu_\beta r_\beta. \tag{28}$$

In this way, instead of computing and storing ${}^jB_{\alpha\beta}$ of size $p\times p$ for each iteration j, we compute and save

q vectors u_α of size p. Note that this algorithm not only avoids building the intermediate matrices $B_{\alpha\beta}$ but also the construction of the final matrix $Q_{\alpha\beta}$ of the QR decomposition. In this way, matrices B in equations 21 and 22 are never completely computed and stored.

3 Results

3.1 Performance comparison

The CIQN algorithm performance was compared against the Aitken (atk) and the Broyden (brd) algorithms. The three relaxation families were tested relaxing the Dirichlet variable (displacement, "d") and the Neumann variable (force, "f"). Also, for the CIQN algorithm, test were made using 5 and 20 previously saved iterations. Figure 2 shows *(a)* a scheme of a test case, *(b)* result for $t = 0.3[s]$ and *(c)* the iterations required to converge the problem in a candle plot. In almost all the cases, the CIQN algorithm performed better than the Aitken or the Broyden algorithms.

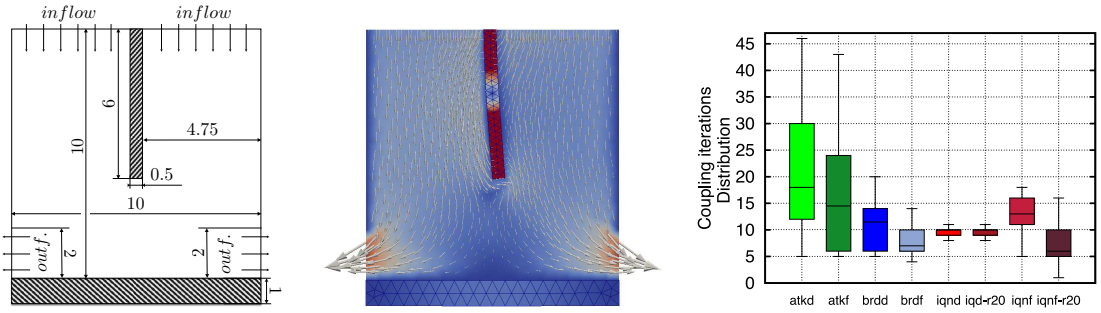

(a) *(b)* *(c)*

Figure 2: *(a)* Scheme of the problem solved. *(b)* Solution at $t = 0.3[s]$. *(c)* Candle bar for the coupling iteration for each relaxation scheme.

in this case, both solid problems are indirectly coupled by the fluid, on which the complexity of the n-field coupling lies. As both interfaces have very different dynamics, the Broyden and CIQN surpass the Aitken algorithm. Both, CIQN and Broyden performs about 60% better than the Aitken. As the Aitken algorithm enforces the Jacobian to be a scalar for all the nodes in the contact surface, it has to increase the iteration number to reach convergence. The difference between Broyden scheme and CIQN scheme is not that notable. Despite CIQN requires 4% more iterations, each iteration is computed 19% faster, probably due to the smaller dispersion between iterations in the CIQN algorithm.

3.2 Fluid-electro-mechanical model of the heart

The geometry used in this example is a modified version of the Zygote Solid 3D heart [36]. This model represents the 50th percentile U.S. 21-year-old Caucasian male. The anatomical description of the heart is completed with a fibre field distribution for the ventricular tissue. In this model, we use a rule-based fibre distribution created with the algorithm described in [37] that is designed with the observations made in [38]. The solid domain mesh has ~ 2.5M tetrahedra and 500k nodes. The fluid domain mesh has ~ 2M tetrahedra and 300k nodes. In both cases, element sizes vary from $100 - 500[\mu m]$, fitting bigger elements in electrically inactive regions. At the wet surface, both meshes' nodes are coincident.

For the electrophysiology problem both ventricular endocardial surfaces are depolarized synchronously, except otherwise stated. For the solid mechanics problem, we propose to use a sliding boundary condition for the pericardial region. This condition restricts the normal displacements $u_i n_i = 0$, while allows tangential displacements $u_i t_i$. Except otherwise specified, the rest of the outer heart and vessels surface is let free ($\sigma_{ij} n_j = 0$). Finally, artery walls are fixed at the end of both the pulmonary trunk and artery arch. For the fluid mechanics problem, we impose open boundary condition on the outflows and no slip velocity condition

$u_i = 0$ on the wet surfaces, where we also enforce continuity of unknowns for the FSI coupling. Results are shown in figure 3, for the fluid-electro-mechanical model solved in the human heart. Q-criterion level surfaces show that the main fluid features occur in the outflow vessels rather than in the intracavitary space as expected. Despite the relatively large endocardial displacements, there are small intraventricular velocities due to the relatively large size of the cavities. On the contrary, the small transversal area in the outflows increase the blood velocity in the vessels.

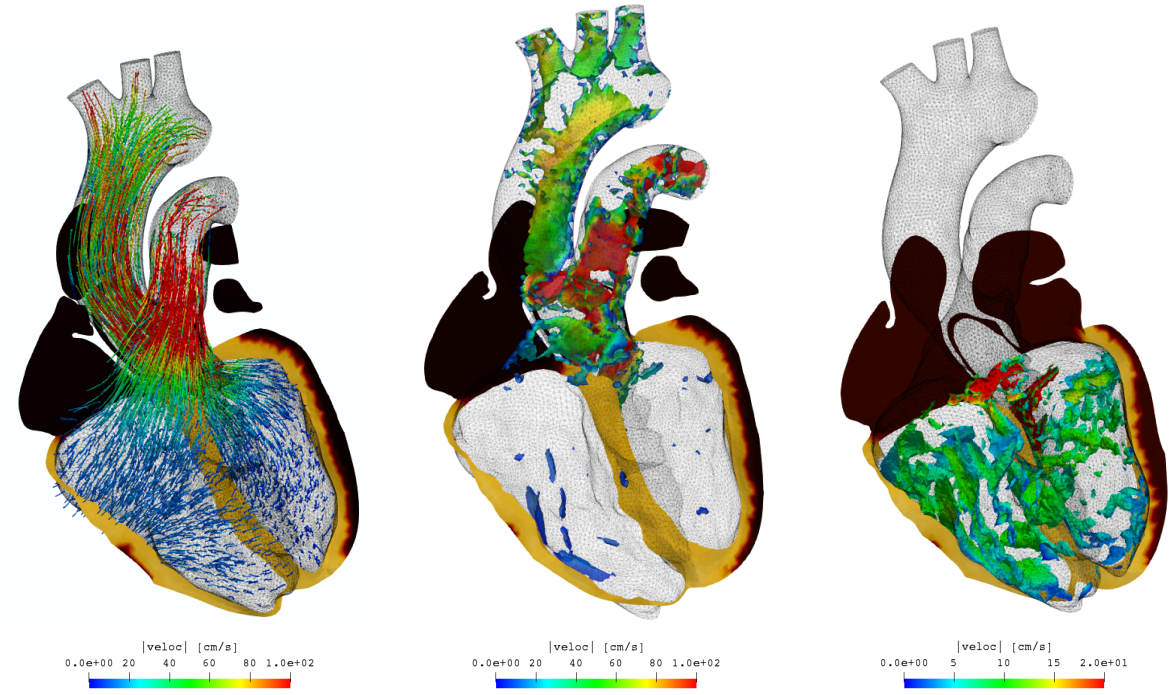

(a) *(b)* *(c)*

Figure 3: Simulation of a heart. In all the images, a long axis slice of the myocardium is seen, representing the electrical depolarization. *(a)* streamlines coloured with velocity magnitude. *(b)* Q-criterion with isosurfaces at $5000[s^-1]$ coloured by velocity magnitude. *(c)* Q-criterion with isosurfaces at $50[s^-1]$ coloured by velocity magnitude.

4 Conclusions

In this work we present an HPC FSI algorithm aimed to tackle the two main problems present in biomechanics: added mass and n-field coupling. These two features are already presented in the original IQN algorithm, being the novelty of this work the HPC implementation. The QR decomposition is fused inside the IQN method to obtain only matrix-vector products and reduce computational and memory consumption. Although this, the algorithm can be improved preconditioning the matrix used for the IQN algorithm to avoid quasi-zero pivots. Also, moving from a Gauss-Seidel scheme (block-serial) to a Jacobi scheme (block-parallel) would reduce even more computational cost and increase the computational efficiency of the algorithm.

This algorithm is used to build a fluid-electro-mechanical model of the human heart. With it, the intracavitary fluid dynamics can be deeply explored. A simple CFD analysis shown that velocities in the outflow tracts are ten times larger compared against the ventricular cavities. A Q-criterion analysis shows that, although vortex are larger in the aorta, the intracavitary patters are more complex.

This work is a step forward building an fluid-electro-mechanical model of the heart. This model allows to obtain a more complete description of the phenomenon which provides a deeper insight in both, the solid and fluid behaviors.

References

[1] Joris Degroote, Klaus Jürgen Bathe, and Jan Vierendeels. Performance of a new partitioned procedure versus a monolithic procedure in fluid-structure interaction. *Computers and Structures*, 87(11-12):793–801, 2009.

[2] Christiane Forster, Wolfgang A. Wall, and Ekkehard Ramm. Artificial added mass instabilities in sequential staggered coupling of nonlinear structures and incompressible viscous flows. *Computer Methods in Applied Mechanics and Engineering*, 196(7):1278–1293, 2007.

[3] Miriam Mehl, Benjamin Uekermann, Hester Bijl, David Blom, Bernhard Gatzhammer, and Alexander Van Zuijlen. Parallel coupling numerics for partitioned fluid-structure interaction simulations. *Computers and Mathematics with Applications*, 71(4):869–891, 2016.

[4] Jane Cioffi. Clinical simulations: Development and validation. *Nurse Education Today*, 21(6):477–486, 2001.

[5] Roger L. Kneebone, W. Scott, A. Darzi, and M. Horrocks. Simulation and clinical practice: Strengthening the relationship. *Medical Education*, 38(10):1095–1102, 2004.

[6] Ahmet Erdemir, Trent M. Guess, Jason Halloran, Srinivas C. Tadepalli, and Tina M. Morrison. Considerations for reporting finite element analysis studies in biomechanics. *Journal of Biomechanics*, 45(4):625–633, 2012.

[7] Irene E. Vignon-Clementel, Alison L. Marsden, and Jeffrey A. Feinstein. A primer on computational simulation in congenital heart disease for the clinician. *Progress in Pediatric Cardiology*, 30(1-2):3–13, 2010.

[8] Y. Qian, J. L. Liu, K. Itatani, K. Miyaji, and M. Umezu. Computational hemodynamic analysis in congenital heart disease: Simulation of the Norwood procedure. *Annals of Biomedical Engineering*, 38(7):2302–2313, 2010.

[9] Theodosios Korakianitis and Yubing Shi. Numerical simulation of cardiovascular dynamics with healthy and diseased heart valves. *Journal of Biomechanics*, 39(11):1964–1982, 2006.

[10] Edward J Vigmond, Clyde Clements, David M. McQueen, and Charles S Peskin. Effect of bundle branch block on cardiac output: A whole heart simulation study. *Progress in Biophysics and Molecular Biology*, 97(2-3):520–542, 2008.

[11] Dalin Tang, Chun Yang, Tal Geva, and Pedro J. del Nido. Image-based patient-specific ventricle models with fluid-structure interaction for cardiac function assessment and surgical design optimization. *Progress in Pediatric Cardiology*, 30(1-2):51–62, 2010.

[12] Ivan Rayment, Hazel M Holden, Michael Whittaker, Christopher B Yohn, Michael Lorenz, Kenneth C Holmes, Ronald A Milligan, Ivan Rayment, Hazel M Holden, Michael Whittaker, Christopher B Yohn, Michael Lorenz, Kenneth C Holmes, and Ronald A Milligan. Structure of the Actin-Myosin Complex and Its Implications for Muscle Contraction. *Science*, 261:58–65, 1993.

[13] S Ebashi and M Endo. Calcium ion and muscle contraction. *Progress in biophysics and molecular biology*, 18:123–183, 1968.

[14] S S Khalafvand, E Y K Ng, and L Zhong. CFD simulation of flow through heart: a perspective review. *Computer methods in biomechanics and biomedical engineering*, 14(1):113–132, 2011.

[15] D A Nordsletten, S A Niederer, M P Nash, P J Hunter, and N P Smith. Coupling multi-physics models to cardiac mechanics. *Progress in Biophysics and Molecular Biology*, 104(1-3):77–88, 2011.

[16] Yanhang Zhang, Victor H. Barocas, Scott A. Berceli, Colleen E. Clancy, David M. Eckmann, Marc Garbey, Ghassan S. Kassab, Donna R. Lochner, Andrew D. McCulloch, Roger Tran-Son-Tay, and Natalia A. Trayanova. Multi-scale Modeling of the Cardiovascular System: Disease Development, Progression, and Clinical Intervention. *Annals of Biomedical Engineering*, 44(9):2642–2660, 2016.

[17] Joris Degroote. Partitioned Simulation of Fluid-Structure Interaction. pages 185–238, 2013.

[18] Gene Hou, Jin Wang, and Anita Layton. Numerical methods for fluid-structure interaction - A review. *Communications in Computational Physics*, 12(2):337–377, 2012.

[19] Guillaume Houzeaux, Mariano Vázquez, R Aubry, and José M Cela. A massively parallel fractional step solver for incompressible flows. *Journal of Computational Physics*, 228(17):6316–6332, 2009.

[20] Mariano Vázquez, Ruth Arís, Guillaume Houzeaux, R Aubry, and P Villar. A massively parallel computational electrophysiology model of the heart. *International journal for numerical methods in biomedical engineering*, 2011.

[21] Mariano Vazquez, Guillaume Houzeaux, Seid Koric, Antoni Artigues, Jazmin Aguado-Sierra, Ruth Aris, Daniel Mira, Hadrien Calmet, Fernando Cucchietti, Herbert Owen, Ahmed Taha, and Jose Maria Cela. Alya: Towards Exascale for Engineering Simulation Codes. pages 1–20, apr 2014.

[22] E. Casoni, a. Jérusalem, C. Samaniego, B. Eguzkitza, P. Lafortune, D. D. Tjahjanto, X. Sáez, G. Houzeaux, and M. Vázquez. Alya: Computational Solid Mechanics for Supercomputers. *Archives of Computational Methods in Engineering*, 2014.

[23] Benjamin Uekermann, Juan Carlos Cajas, Bernhard Gatzhammer, Guillaume Houzeaux, Miriam Mehl, and Mariano Vazquez. Towards Partitioned Fluid-Structure Interaction on Massively Parallel Systems. *11th World Congress on Computational Mechanics (WCCM XI)*, (Wccm Xi):1–12, 2014.

[24] Richard FitzHugh. Impulses and physiological states in theoretical models of nerve membrane. *Biophysical journal*, (1948), 1961.

[25] Flavio H Fenton and Alain Karma. Vortex dynamics in three-dimensional continuous myocardium with fiber rotation: Filament instability and fibrillation. *Chaos (Woodbury, N.Y.)*, 8(4):879, dec 1998.

[26] K H W J Ten Tusscher and A V Panfilov. Cell model for efficient simulation of wave propagation in human ventricular tissue under normal and pathological conditions. *Physics in Medicine and Biology*, 51(23):6141–56, 2006.

[27] Alfonso Bueno-Orovio, Elizabeth M. Cherry, and Flavio H. Fenton. Minimal model for human ventricular action potentials in tissue. *Journal of Theoretical Biology*, 253(3):544–560, 2008.

[28] Thomas O'Hara, László Virág, András Varró, and Yoram Rudy. Simulation of the undiseased human cardiac ventricular action potential: Model formulation and experimental validation. *PLoS Computational Biology*, 7(5), 2011.

[29] J.D. Humphrey. Continuum biomechanics of soft biological tissues. *Proc. R. Soc. Lond.*, 459:3–46, 2002.

[30] Gerhard a Holzapfel and Ray W Ogden. Constitutive modelling of passive myocardium: a structurally based framework for material characterization. *Philosophical transactions. Series A, Mathematical, physical, and engineering sciences*, 367(1902):3445–75, 2009.

[31] P.J. Hunter, a.D. McCulloch, and H.E.D.J. ter Keurs. Modelling the mechanical properties of cardiac muscle. *Progress in Biophysics and Molecular Biology*, 69(2-3):289–331, mar 1998.

[32] G. Houzeaux and J. Principe. A variational subgrid scale model for transient incompressible flows. *International Journal of Computational Fluid Dynamics*, 22(3):135–152, 2008.

[33] Ramon Calderer and Arif Masud. A multiscale stabilized ALE formulation for incompressible flows with moving boundaries. *Computational Mechanics*, 46(1):185–197, 2010.

[34] Ulrich Küttler and Wolfgang A. Wall. Fixed-point fluid-structure interaction solvers with dynamic relaxation. *Computational Mechanics*, 43(1):61–72, 2008.

[35] C. G. Broyden. A Class of Methods for Solving Nonlinear Simultaneous Equations. *Mathematics of Computation*, 19(92):577, 1965.

[36] Zygote Media Group Inc. Zygote Solid 3D heart Generation II Developement Report. Technical report, 2014.

[37] Mark Potse, Bruno Dubé, and Alain Vinet. A comparison of monodomain and bidomain propagation models for the human heart. *Annual International Conference of the IEEE Engineering in Medicine and Biology - Proceedings*, 53(12):3895–3898, 2006.

[38] Daniel D. Streeter and David L. Bassett. An engineering analysis of myocardial fiber orientation in pig's left ventricle in systole. *The Anatomical Record*, 155(4):503–511, 1966.